

# NRFormer: Nationwide Nuclear Radiation Forecasting with Spatio-Temporal Transformer

Tengfei Lyu

The Hong Kong University of Science  
and Technology (Guangzhou)  
tlyu077@connect.hkust-gz.edu.cn

Jindong Han

The Hong Kong University of Science  
and Technology  
jhanao@connect.ust.hk

Hao Liu\*

The Hong Kong University of Science  
and Technology (Guangzhou)  
The Hong Kong University of Science  
and Technology  
liuh@ust.hk

## ABSTRACT

Nuclear radiation, which refers to the energy emitted from atomic nuclei during decay, poses significant risks to human health and environmental safety. Recently, advancements in monitoring technology have facilitated the effective recording of nuclear radiation levels and related factors, such as weather conditions. The abundance of monitoring data enables the development of accurate and reliable nuclear radiation forecasting models, which play a crucial role in informing decision-making for individuals and governments. However, this task is challenging due to the imbalanced distribution of monitoring stations over a wide spatial range and the non-stationary radiation variation patterns. In this study, we introduce NRFormer, a novel framework tailored for the nationwide prediction of nuclear radiation variations. By integrating a non-stationary temporal attention module, an imbalance-aware spatial attention module, and a radiation propagation prompting module, NRFormer collectively captures complex spatio-temporal dynamics of nuclear radiation. Extensive experiments on two real-world datasets demonstrate the superiority of our proposed framework against 11 baselines. NRFormer has been deployed online to provide 1–24-day nuclear radiation forecasts, empowering individuals and governments with timely, data-driven decisions for emergency response and public safety. Our framework is designed for general applicability and can be readily adapted for deployment in other regions. The deployed system is available at <https://NRFormer.github.io> and the dataset and code of the predictive model are available at <https://github.com/usail-hkust/NRFormer>.

## KEYWORDS

nuclear radiation forecasting system, spatio-temporal modeling, imbalance-aware transformer

\*Corresponding author.

Permission to make digital or hard copies of all or part of this work for personal or classroom use is granted without fee provided that copies are not made or distributed for profit or commercial advantage and that copies bear this notice and the full citation on the first page. Copyrights for components of this work owned by others than ACM must be honored. Abstracting with credit is permitted. To copy otherwise, or republish, to post on servers or to redistribute to lists, requires prior specific permission and/or a fee. Request permissions from [permissions@acm.org](mailto:permissions@acm.org).

Conference'17, July 2017, Washington, DC, USA

© 2025 Association for Computing Machinery.  
ACM ISBN 978-x-xxxx-xxxx-x/YY/MM...\$15.00  
<https://doi.org/10.1145/nnnnnnn.nnnnnnn>

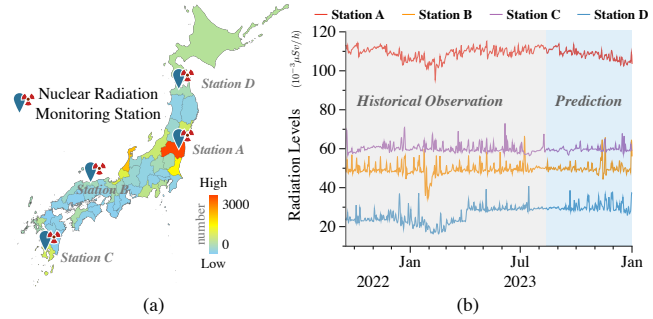


**Figure 1: Collaborative nuclear radiation forecasting for nationwide stations in Japan. (a) Spatial distribution of monitoring stations in Japan, high-risk areas (i.e., with more nuclear power plants) have more stations. (b) Time-varying radiation levels at different monitoring stations.**

## ACM Reference Format:

Tengfei Lyu, Jindong Han, and Hao Liu. 2025. NRFormer: Nationwide Nuclear Radiation Forecasting with Spatio-Temporal Transformer. In *Proceedings of ACM Conference (Conference'17)*. ACM, New York, NY, USA, 12 pages. <https://doi.org/10.1145/nnnnnnn.nnnnnnn>

## 1 INTRODUCTION

Nuclear power is recognized as a clean and economical energy source and has been a part of global energy for more than 50 years. However, the potential leakage of nuclear radioactive material poses significant threats to environmental and public safety. Severe nuclear disasters, such as the Chernobyl accident in the Soviet Union [1] and the Fukushima accident in Japan [38], have underscored the far-reaching and long-lasting impacts of nuclear radiation across vast geographical areas, affecting diverse ecosystems and public health. In response, numerous countries have established monitoring stations to track nuclear radiation levels (e.g., gamma rays) in the environment. Beyond real-time monitoring, there is an increasing demand for predictive modeling of future radiation level variations. Accurate radiation forecasting can substantially reduce potential socio-economic losses by enabling timely precautionary measures, such as containment of radioactive contamination, evacuation planning, and distribution of protective equipment.

In this paper, we study the national-wide nuclear radiation forecasting problem, which involves collaborative forecasting across distributed monitoring stations throughout the country. Figure 1 shows an illustrative example of radiation forecasting in Japan. The dispersion of nuclear radiation is primarily influenced by the global circulation system (i.e., atmospheric and ocean circulation) [33],

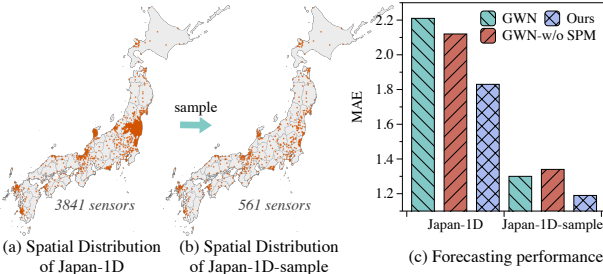


**Figure 2: Empirical study of the imbalanced spatial distribution problem. (1) Full station distribution of our constructed Japan-1D dataset. (2) Evenly sampled station distribution (from Japan-1D dataset). (3) The forecasting performance of GWN on Japan datasets, where GWN-w/o SPM is the model variant that removes the spatial propagation module (SPM).**

manifesting intricate spatio-temporal patterns. Therefore, an effective forecasting model must be capable of comprehending these spatio-temporal correlations from geo-distributed stations. Recent advances in Spatio-Temporal Graph Neural Networks (STGNNs) [18, 23, 36, 37, 46, 54], which combine Graph Neural Networks (GNNs) with sequential models (e.g., RNN), have shown superiority in various applications such as traffic forecasting [2, 47] and air quality prediction [13]. Nonetheless, existing STGNNs often fall short in capturing the complex dynamics of nuclear radiation, primarily due to the following three major challenges.

**Challenge 1: Non-stationary temporal patterns.** The nuclear radiation variability is typically driven by unpredictable events like irregular human interventions or nuclear power plant leakages, exhibiting a highly non-stationary nature. This means the statistical properties (e.g., mean and variance) and the underlying distribution of radiation series is shifting over time. Traditional STGNNs, which rely on Convolution Neural Networks (CNNs) or Recurrent Neural Networks (RNNs) for temporal pattern preservation [34], may struggle to effectively model these erratic, non-stationary properties, thereby affecting predictability. How to mitigate the non-stationary effect towards better predictability is the first challenge.

**Challenge 2: Imbalanced spatial distribution.** Radiation monitoring stations are often deployed unevenly, with dense clusters near nuclear facilities and sparse distribution in other regions. Typical STGNNs capture spatial correlations by representing these stations as graph nodes and propagating information between adjacent nodes. However, such an approach is less effective in scenarios with spatial imbalances, as nodes in densely populated regions tend to be easily overwhelmed by abundant information, while sparsely connected nodes in other areas fail to perceive sufficient spatial context for prediction. For instance, we illustrate our insights using GWN [47], a widely adopted spatio-temporal model. As reported in Figure 2, we observe that removing the spatial propagation module of GWN (i.e., GWN-w/o SPM) diminished forecasting effectiveness on a balanced subset, whereas the opposite results are observed when using the full dataset. Such results indicate that the utility of the graph learning module is compromised, leading to reduced accuracy in datasets with significant spatial imbalances. Consequently, how to capture diversified dependencies from uneven spatial distribution is also a critical challenge.

**Challenge 3: Heterogeneous contextual factors.** The variation of radiation levels at each station is also influenced by a variety of contextual factors, including meteorological conditions, terrain variations, and significant events. These factors may interact with each other, jointly affecting the path and intensity of nuclear radiation. How to effectively incorporate heterogeneous contextual factors is imperative for improving the accuracy and reliability of the predictive model.

To address the above challenges, we introduce NRFormer, a spatio-temporal graph Transformer network for national-wide nuclear radiation forecasting. Our approach is motivated by the recent success of Transformer [40] in modeling complex data dependencies through an attention mechanism. Specifically, we first devise a non-stationary temporal attention module, which addresses the distribution shift in radiation time series by integrating instance-level normalization into point-wise temporal attention. After that, we propose an imbalance-aware spatial attention module to selectively absorb spatial knowledge for nodes with extremely dense and scarce neighborhoods, thus alleviating the spatial imbalance challenge. Moreover, we develop a radiation propagation prompting strategy to guide the predictive modeling process. The prompts not only inject context-specific knowledge into our model for better radiation propagation but also enable robust generalization in unseen scenarios. Our contributions are summarized as follows:

- We investigate the nationwide nuclear radiation forecasting problem. To the best of our knowledge, this is the first work to collectively predict radiation on a national scale.
- We propose NRFormer, a predictive model specifically designed to address distinct challenges in nuclear radiation forecasting. By integrating a non-stationary temporal attention module, an imbalance-aware spatial attention module, and a radiation propagation prompting module, NRFormer effectively captures complex spatio-temporal dynamics inherent to nuclear radiation phenomena.
- We construct two large-scale nuclear radiation datasets named Japan-4H and Japan-1D, encompassing three years of nuclear radiation data from 3,841 monitoring stations across Japan. We release the dataset<sup>1</sup> to facilitate future research in this area. Extensive experiments validate the effectiveness of NRFormer against 11 baselines.
- We deploy a web-based, real-time radiation forecasting system<sup>2</sup>, providing 1–24-day predictions and rich radiation data analysis, while offering interactive insights into spatial-temporal radiation patterns.

## 2 PRELIMINARIES

**DEFINITION 1. *Radiation level.*** *Radiation level is a number used to quantify the concentrations of radioactive materials in the environment. A higher radiation level indicates that people will experience increasingly detrimental health effects. In practice, the radiation level is computed by using the weighted sum of several radioactive substance measurements, including alpha particles, beta particles, neutron particles, and gamma rays.*

<sup>1</sup><https://github.com/usail-hkust/NRFormer>

<sup>2</sup><https://NRFormer.github.io>

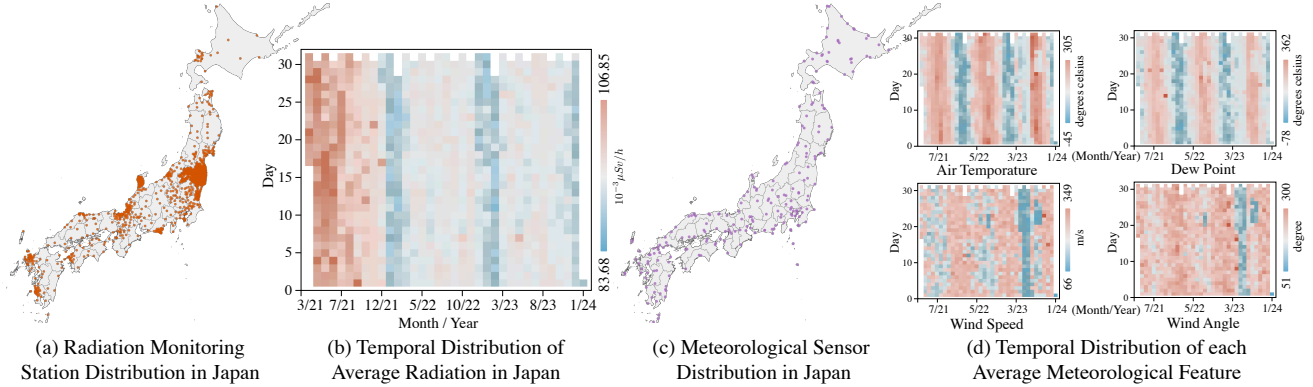


**Figure 3: Distributions of the radiation and meteorological datasets: (a) spatial distribution of radiation monitoring stations; (b) temporal distribution of daily average radiation in Japan; (c) spatial distribution of meteorological stations; (d) temporal distribution of the daily average value of each meteorological station across Japan.**

**DEFINITION 2. Radiation monitoring network.** The radiation monitoring network consists of a group of monitoring stations, denoted as  $\mathcal{G} = (V, E)$ , where  $V$  is a set of stations and  $N = |V|$  is the number of stations,  $E$  denotes a set of edges representing the relationships among stations. Here we use  $A \in \mathbb{R}^{N \times N}$  to denote the adjacency matrix of the monitoring network.

To build  $\mathcal{G}$ , we compute the pairwise distances between stations and derive the adjacency matrix using a pre-defined distance threshold. Let  $X \in \mathbb{R}^{T \times N}$  be the observed radiation level from all stations, where  $T$  is the number of time steps. We use  $C \in \mathbb{R}^{T \times N \times C}$  to denote the contextual features associated with each station, e.g., meteorological and location information, where  $C$  is the feature dimension. Let  $\mathcal{H}^t = (\mathcal{G}, X^t, C^t)$  indicates all the observed values at time step  $t$ , we define the problem as follows.

**PROBLEM STATEMENT. Nuclear radiation forecasting.** Given the radiation monitoring network  $\mathcal{G}$ , historical radiation levels  $X$ , contextual features  $C$ , the goal is to predict the radiation level for all the monitoring stations over the next  $K$  time steps:

$$(\hat{Y}^{t+1}, \hat{Y}^{t+2}, \dots, \hat{Y}^{t+K}) \leftarrow \mathcal{F}_\theta(\mathcal{H}^{t-P+1}, \mathcal{H}^{t-P+2}, \dots, \mathcal{H}^t), \quad (1)$$

where  $\hat{Y}^{t+K}$  denotes the predicted value at time step  $t + K$ ,  $\mathcal{F}_\theta$  is the forecasting model,  $P$  and  $K$  are the number of historical and future time steps, respectively.

### 3 SYSTEM OVERVIEW

#### 3.1 System Architecture

Figure 4 illustrates the architecture of our deployed radiation forecasting system. The *Data Sources* consist of publicly accessible web services that provide real-time radiation and meteorological data. The *Data Collector* systematically acquires time-series data from external sources through web-service APIs or automated web-scraping techniques. During the *Data Processing* and *Data Analysis* stages, raw data are cleaned and stored in a cloud-based database. The *Predictive Model* leverages this refined dataset to generate forecasts of radiation levels for each radiation monitoring station over the next 1 to 24 days. These forecasts are stored in the cloud database and retrieved by the *Web Service*, which provides access to forecasting results and enables interactive visualization and analysis of radiation data through dynamic web interfaces.

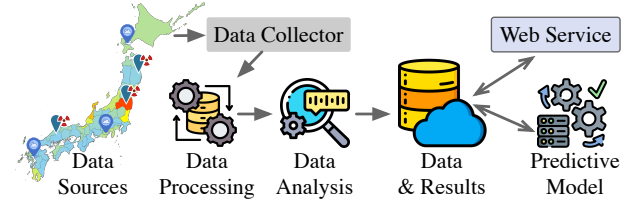


**Figure 4: Architecture of deployed forecasting system.**

#### 3.2 Data Collecting and Processing

**Nuclear radiation data.** The nuclear radiation data are continuously collected from Japan's Nuclear Regulation Authority <sup>3</sup>, consisting of 10-minute interval radiation measurements from over 4,000 monitoring stations. Stations with more than 30 days of missing data were excluded, resulting in a refined dataset of 3,841 stations. To analyze radiation forecasting from both long-term and short-term perspectives, the original data were preprocessed to generate two datasets: (1) *Japan-4H*, comprising 4-hour averaged values, and (2) *Japan-1D*, containing daily averaged values.

**Meteorological data.** Considering the significant influence of meteorological conditions on the spread of radiation, we continuously collect Integrated Surface Dataset (ISD) from the National Oceanic and Atmospheric Administration (NOAA) <sup>4</sup>. The ISD dataset includes hourly surface meteorological observations from over 35,000 weather stations worldwide, covering a variety of parameters like pressure, temperature, dew point, winds, and so on. By using the geographic coordinates, we identify 235 weather stations in Japan and match them to corresponding radiation monitoring stations. We extract key meteorological variables, including wind speed, wind direction, air temperature, and dew point, as contextual features for radiation forecasting task.

#### 3.3 Data Analysis

To investigate radiation distribution patterns, we perform a preliminary analysis of radiation and meteorological data, as illustrated in Figure 3. First, Figures 3(a) and 3(c) visualize the spatial distributions of radiation and weather stations, respectively. The analysis

<sup>3</sup><https://www.erns.nsr.go.jp/nra-ramis-webg/>

<sup>4</sup><https://www.noaa.gov/metadata/geoportal/rest/metadata/item/gov.noaa.ncdc:C00532/html>

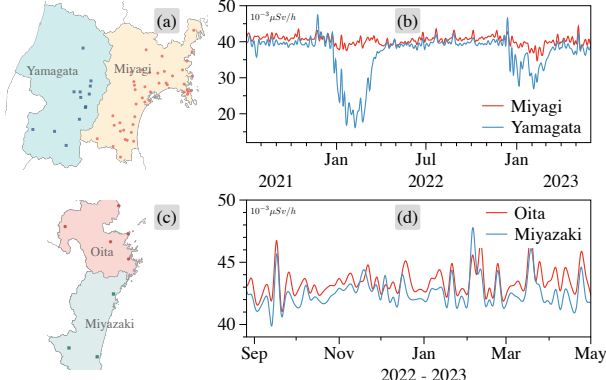


**Figure 5: Comparison of radiation patterns in adjacent prefectures, which demonstrates that radiation patterns in neighboring areas can be either very similar or quite dissimilar. (a) and (c) shows the geographical distribution of radiation stations. (b) and (d) present the variation of average radiation levels in corresponding prefectures.**

reveals a highly skewed spatial distribution of radiation stations, *i.e.*, dense clustering near high-risk nuclear facilities. Figure 3(b) displays the temporal distribution of average radiation levels, showing a pronounced downward trend beginning March 17, 2021, with January exhibiting the lowest annual levels—a pattern potentially linked to seasonal meteorological conditions.

We further analyze spatial and temporal distributions across adjacent prefectures in Figure 5, which demonstrates significant non-linear variations in radiation levels across both dimensions. Notably, radiation patterns in geographically proximate regions are not necessarily more similar than those in distant areas, likely due to external complexities such as unpredictable human activities. These dynamics complicate the modeling of spatio-temporal correlations, particularly for densely clustered monitoring stations.

Additionally, we empirically examine relationships between meteorological factors and radiation levels. Figure 3(d) illustrates the temporal distributions of four meteorological variables: wind speed, wind direction, air temperature, and dew point. Temperature and dew point exhibit daily patterns strongly correlated with radiation trends in Figure 3(b). While wind parameters lack explicit correlations, their potential implicit influence on radiation propagation justifies their inclusion. This analysis confirms statistically significant relationships between meteorological conditions and radiation levels, with their integration substantially improving accuracy.

### 3.4 User Interfaces

We developed a web-based real-time forecasting system to provide nationwide radiation level predictions across Japan. The deployed system is presented in Figure 10 and 11 in the Appendix and available at <https://NRFormer.github.io>.

This deployed system enables users to monitor temporal changes in radiation levels. As shown in Figure 10, each monitoring station is represented by a blue marker on the map. Selecting a station triggers a pop-up chart that depicts forecasted radiation levels for subsequent days, offering insights into projected radiation trends.

These visualizations assist stakeholders in environmental and public health risk assessment and mitigation planning. Additionally, Figure 10 features a heatmap displaying daily radiation forecasts across Japan. The heatmap highlights geospatial variations in radiation levels, revealing patterns and dispersion dynamics over time. This enables policymakers to identify regional disparities and temporal progression of radiation exposure risks.

As illustrated in Figure 11, the system provides multifaceted radiation analysis through multiple visualization modalities. This system allows both individuals and government agencies to examine radiation data from diverse perspectives, fostering a holistic comprehension of nuclear risks and supporting data-driven decision-making processes.

## 4 THE PREDICTIVE MODEL

**Overview.** The framework of NRFormer is shown in Figure 6, which is comprised of three modules: (1) *The Non-stationary Temporal Attention*: it integrates instance-wise normalization into point-wise temporal attention to capture the non-stationary dynamics of radiation. (2) *The Imbalance-aware Spatial Attention*: it models both macro-scale and proximity-constrained spatial dependencies to selectively propagate spatial knowledge for nodes with extremely dense or sparse neighborhoods. (3) *The Radiation Propagation Prompting*: it utilizes contextual features to provide a contextual prompt for the imbalanced-aware spatial attention module, enhancing prediction with essential environmental and spatial insights. Finally, the output layer fuses the embeddings from temporal and spatial attention, and then denormalizes them to produce the final prediction results. Next, we present each component in detail.

### 4.1 Non-stationary Temporal Attention

As depicted in Figure 4, the radiation time series often showcase a highly non-stationary nature. To effectively extract stable knowledge from radiation sequence inputs, we first introduce the non-stationary temporal attention, which consists of two parts: non-stationary normalization and point-wise temporal attention.

**4.1.1 Non-stationary normalization.** Due to the non-stationarity of radiation time series, the underlying distributions of different input sequences are diverse, which significantly degrades the forecasting performance. Motivated by recent works [20, 31], we aim to eliminate the non-stationary information in each input sequence by using instance-wise normalization.

Formally, given historical observations  $\mathbf{x}_i \in \mathbb{R}^P$  at  $i$ -th station, where  $P$  is the input time window. We first calculate the mean and variance of each input sequence  $\mathbf{x}_i$  as follows:

$$\mathbb{E}[\mathbf{x}_i] = \frac{1}{P} \sum_{j=1}^P \mathbf{x}_i^j, \quad \text{Var}[\mathbf{x}_i] = \frac{1}{P} \sum_{j=1}^P (\mathbf{x}_i^j - \mathbb{E}[\mathbf{x}_i])^2, \quad (2)$$

where  $\mathbb{E}[\cdot]$  and  $\text{Var}[\cdot]$  are the mean and variance function, respectively. After that, we leverage  $\mathbb{E}[\mathbf{x}_i]$  and  $\text{Var}[\mathbf{x}_i]$  to normalize the original input sequence  $\mathbf{x}_i$ , defined as

$$\hat{\mathbf{x}}_i = \gamma_i \frac{\mathbf{x}_i - \mathbb{E}[\mathbf{x}_i]}{\sqrt{\text{Var}[\mathbf{x}_i] + \epsilon}} + \beta_i, \quad (3)$$

where  $\gamma_i$  and  $\beta_i$  are learnable parameters corresponding to the  $i$ -th station, and  $\epsilon$  is a small value that ensures numerical stability.

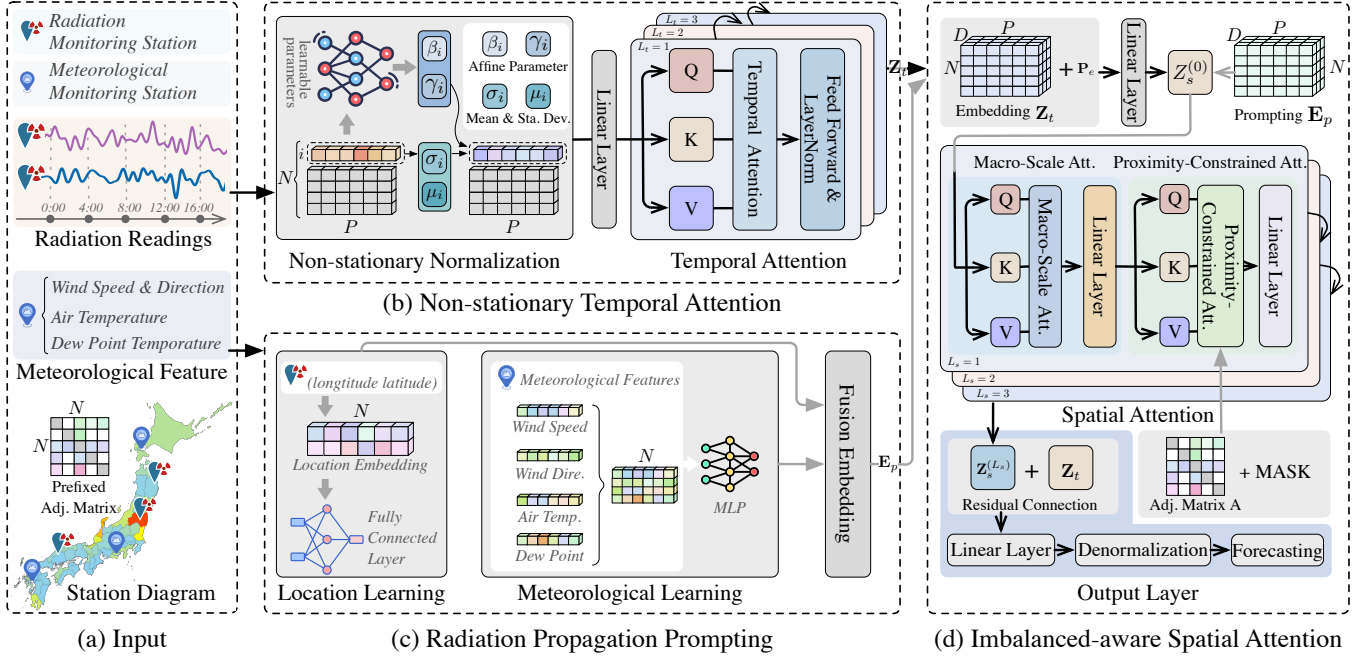


Figure 6: The framework overview of NRFormer.

Intuitively, the normalized sequences possess more stable statistical properties, which largely reduce the difficulty of capturing temporal dynamics within the non-stationary data. Subsequently, we process  $\hat{x}_i$  through an embedding layer:  $\mathbf{z}_t^i = \text{Embed}(\hat{x}_i)$ , where  $\mathbf{z}_t^i \in \mathbb{R}^{P \times D}$  represents the point-wise time series embedding of station  $i$  that will be fed into subsequent temporal attention module,  $D$  is the hidden dimension of each time step.

**4.1.2 Point-wise temporal attention.** Many STGNNs [18] rely on CNNs or RNNs to capture the dependencies among different time steps. However, these models may not be able to capture unstable and long-range temporal dependencies, both of which appear in nuclear radiation time series. We address this issue by utilizing a point-wise temporal attention module.

Concretely, we follow the terminology in [40] and leverage *query*, *key*, and *value* to indicate the intermediate representation vectors in self-attention mechanism. Given embedding  $\mathbf{z}_t^i$ , we derive the *query*, *key*, and *value* matrices by using the following equations:

$$\mathbf{Q}_t = \mathbf{z}_t^i \mathbf{W}_t^Q, \quad \mathbf{K}_t = \mathbf{z}_t^i \mathbf{W}_t^K, \quad \mathbf{V}_t = \mathbf{z}_t^i \mathbf{W}_t^V, \quad (4)$$

where  $\mathbf{W}_t^Q, \mathbf{W}_t^K, \mathbf{W}_t^V \in \mathbb{R}^{D \times D}$  are learnable parameters shared across different stations and time steps. Afterward, we compute attention score  $\mathbf{A}_t$  to measure relationships among any two time steps,  $\mathbf{A}_t = \frac{\mathbf{Q}_t \mathbf{K}_t^\top}{\sqrt{D}}$ , where  $\mathbf{A}_t \in \mathbb{R}^{P \times P}$  and  $\sqrt{D}$  is the scaling factor.

We normalize each row of  $\mathbf{A}_t$  with a Softmax function, and obtain the updated representation vector as follows  $\mathbf{z}_t^{i,(l)} = \text{Softmax}(\mathbf{A}_t) \mathbf{V}_t$ . To enhance the effectiveness of temporal dependency modeling, we further equip multi-head attention and residual connection technique for each layer, followed by layer normalization [40]. We build the temporal attention module by stacking  $L_t$  such layers, and denote the output of the  $L_t$ -th layer as  $\mathbf{z}_t^{i,(L_t)}$ .

Finally, we flatten  $\mathbf{z}_t^{i,(L_t)}$  into a 1D vector and map the flattened version into a hidden representation,  $\mathbf{z}_t^i = \text{Flatten}(\mathbf{z}_t^{i,(L_t)}) \mathbf{W}^r$ , where  $\mathbf{W}^r$  is learnable parameters. Let  $\mathbf{Z}_t \in \mathbb{R}^{N \times D}$  denotes the hidden representations of all the nodes (*i.e.*, stations), where the  $i$ -th row vector of  $\mathbf{Z}_t$  is  $\mathbf{z}_t^i$ .

## 4.2 Imbalance-aware Spatial Attention

As previously mentioned, the nodes in dense clusters have the risk of information overload (*i.e.*, over-smoothing) and sparsely connected nodes have the risk of information insufficient (*i.e.*, under-smoothing) in spatial dependency modeling, leading to sub-optimal performance. To alleviate this problem, we develop the imbalance-aware spatial attention, which includes two parts: (1) a macro-scale spatial correlation modeling module to enrich the spatial neighborhood of orphan nodes, and (2) a proximity-constrained spatial modeling module to reduce the influence of noisy neighborhood for densely connected nodes.

Following previous works [22, 40], we add positional encoding into  $\mathbf{Z}_s$  to preserve critical spatial information of each node:  $\mathbf{Z}_s^{(0)} = \mathbf{Z}_t + \mathbf{P}_e$ , where  $\mathbf{P}_e \in \mathbb{R}^{N \times D}$  is a learnable positional embedding matrix. The resulting matrix  $\mathbf{Z}_s^{(0)}$  will be fed into the following spatial attention block for spatial dependency modeling.

**4.2.1 Macro-Scale Spatial Correlation Modeling.** In this part, we employ the macro-scale spatial attention mechanism to identify latent neighborhoods for sparsely-connected nodes. Specifically, we first compute the attention score between arbitrary nodes:

$$\mathbf{Q}_g = \mathbf{Z}_s^{(0)} \mathbf{W}_g^Q, \quad \mathbf{K}_g = \mathbf{Z}_s^{(0)} \mathbf{W}_g^K, \quad \mathbf{V}_g = \mathbf{Z}_s^{(0)} \mathbf{W}_g^V, \quad (5)$$

$$\mathbf{A}_g = \frac{\mathbf{Q}_g \cdot \mathbf{K}_g^\top}{\sqrt{D}}, \quad (6)$$

where  $\mathbf{A}_g \in \mathbb{R}^{N \times N}$  is the attention score matrix that encodes the all-pair node relationships. Then, we can propagate node signals based on the normalized  $\mathbf{A}_g$ , defined as  $\mathbf{H}_g = \text{Softmax}(\mathbf{A}_g) \cdot \mathbf{V}_g$ . Next, we further adopt a feed-forward layer to enhance the model expressive capabilities,  $\mathbf{H}'_g = (\text{ReLU}(\mathbf{H}_g \cdot \mathbf{W}_1 + \mathbf{b}_1)) \cdot \mathbf{W}_2 + \mathbf{b}_2$ , where  $\mathbf{W}_1, \mathbf{W}_2$  are the learnable matrices and  $\mathbf{b}_1, \mathbf{b}_2$  are the bias parameters. In summary, macro-scale spatial attention can provide additional spatial information for nodes with scarce neighborhoods, which reduces the risk of under-smoothing phenomena.

**4.2.2 Proximity-Constrained Spatial Correlation Modeling.** In practice, the macro-scale spatial attention may introduce massive noises for densely-connected nodes via all-pair message passing, which exacerbates the over-smoothing issue. Therefore, we devise proximity spatial attention by adding a graph constraint to filter those neighbors that are far away from the target nodes. Likewise, we first compute the attention score matrix  $\mathbf{A}_l$  and the key matrix  $\mathbf{V}_l$  via Equations 5 and 6. Suppose  $\mathbf{A}$  denotes the truncated adjacency matrix built from geographical distance, we define a masked matrix  $\mathbf{A}_{mask}$  based on  $\mathbf{A}$  and  $\mathbf{A}_l$ :

$$\mathbf{A}_{mask}[i, j] = \begin{cases} \mathbf{A}_l[i, j], & \text{if } \mathbf{A}[i, j] > 0 \\ -\infty, & \text{otherwise} \end{cases} \quad (7)$$

where  $\mathbf{A}_{mask}[i, j]$  is set to  $-\infty$  if the distance between node  $i$  and  $j$  exceeds a threshold. Afterwards, we perform spatial message passing under proximity constraint:  $\mathbf{H}_l = \text{Softmax}(\mathbf{A}_{mask}) \cdot \mathbf{V}_l$ . The output  $\mathbf{H}_l$  is then fed into a feed-forward layer,

$$\mathbf{H}'_l = (\text{ReLU}(\mathbf{H}_l \cdot \mathbf{W}_3 + \mathbf{b}_3)) \cdot \mathbf{W}_4 + \mathbf{b}_4, \quad (8)$$

where  $\mathbf{W}_3, \mathbf{W}_4$  are the learnable matrices and  $\mathbf{b}_3, \mathbf{b}_4$  are the bias parameters. The proximity spatial message passing operator can restrict the spatial receptive field of densely connected nodes and enable the adaptive selection of useful neighboring nodes, which can avoid potential over-smoothing risk. We alternately stack  $L_s$  macro-scale and proximity spatial attention layers for spatial dependency modeling. The final output is denoted as  $\mathbf{Z}_s^{(L_s)}$ .

### 4.3 Radiation Propagation Prompting

Considering the significant impact of context factors on radiation propagation, we encode context-specific knowledge as prompts to guide model forecasting. In particular, we incorporate two types of prompts: the location prompt and the meteorological prompt.

**Location prompt.** Different locations in geographical space often exhibit distinct spatial characteristics, which could potentially affect the spread of radioactive materials. To implicitly capture this critical feature, we introduce the geographical coordinates of each radiation monitoring station, denoted as  $\mathbf{L} \in \mathbb{R}^{N \times C_g}$ , where  $N$  represents the number of stations and  $C_g = 2$  is feature dimension, *i.e.*, longitude and latitude. We project  $\mathbf{L}$  into a latent embedding space via an embedding layer, and apply Multi-Layer Perceptron (MLP) to fuse the embeddings, defined as  $\mathbf{E}_l = \text{MLP}_l(\text{Embed}(\mathbf{L}))$ .

**Meteorological prompt.** Meteorological conditions significantly influence the spatial propagation of nuclear radiation. For example, strong wind can carry radioactive material over long distances, affecting areas far from the contamination source. Therefore, for each radiation monitoring station, we retrieve the observations of its nearest meteorological station as prompt features, denoted as

$\mathbf{M} \in \mathbb{R}^{N \times T \times C_m}$ , where  $C_m$  is the number of meteorological features. We flatten the last two dimensions of  $\mathbf{M}$  into a 2D matrix  $\mathbf{M}' \in \mathbb{R}^{N \times C_o}$ , where  $C_o = T \times C_m$ . Similarly, we transform the raw features into a latent feature representation through an MLP:  $\mathbf{E}_m = \text{MLP}_m(\mathbf{M}')$ . After that, we fuse the above two prompt feature vectors  $\mathbf{E}_p = \mathbf{E}_l || \mathbf{E}_m$ , where  $\mathbf{E}_p$  is the contextual prompt embedding that will be injected into the imbalanced-aware spatial attention as addition clues. Concretely, we can rewrite Equation 5 as

$$\mathbf{Q}_g = (\mathbf{Z}_s^{(0)} || \mathbf{E}_p) \mathbf{W}_g^Q, \mathbf{K}_g = (\mathbf{Z}_s^{(0)} || \mathbf{E}_p) \mathbf{W}_g^K, \mathbf{V}_g = \mathbf{Z}_s^{(0)} \mathbf{W}_g^V. \quad (9)$$

Overall, the prompting strategy enables our model to take the complex interplay between geographical location and meteorology into account in radiation propagation modeling.

### 4.4 Output Layer

To make predictions, we concatenate the embedding  $\mathbf{Z}_t$  and  $\mathbf{Z}_s^{(L_s)}$ , and then feed it into fully connected layers. The formulation is shown as follows:

$$\tilde{\mathbf{Y}}^{t+1:t+K} = ((\mathbf{Z}_t || \mathbf{Z}_s^{(L_s)}) \cdot \mathbf{W}_i + \mathbf{b}_i) \cdot \mathbf{W}_o + \mathbf{b}_o, \quad (10)$$

where  $\mathbf{W}_i$  and  $\mathbf{W}_o$  are the learnable matrices, and  $\mathbf{b}_i$  and  $\mathbf{b}_o$  are the bias parameters. Suppose  $\tilde{\mathbf{y}}^i \in \mathbb{R}^K$  represents the  $i$ -th row vector of  $\tilde{\mathbf{Y}}^{t+1:t+K}$ , we denormalize the model output  $\tilde{\mathbf{y}}_i$  using the reciprocal of the instance normalization, denoted as

$$\hat{\mathbf{y}}_i = \sqrt{\text{Var}[\mathbf{x}^{(i)}] + \epsilon} \cdot \frac{\tilde{\mathbf{y}}_i - \beta_i}{\gamma_k} + \mathbb{E}[\mathbf{x}^{(i)}], \quad (11)$$

where  $\hat{\mathbf{y}}_i$  denotes the future prediction of station  $i$ . Finally, we aim to optimize the following objective:  $\mathcal{L} = \frac{1}{N} \sum_{i=1}^N |\hat{\mathbf{y}}_i - \mathbf{y}_i|$ , where  $\mathbf{y}_i$  is the ground truth radiation level of station  $i$ .

## 5 EXPERIMENTS

In this section, we introduce the experiment setup, overall performance, ablation study, and deployed system evaluation. Due to the page limit, we report the details of parameter sensitivity analysis in Appendix A.3.

### 5.1 Experiments Setup

**5.1.1 Datasets.** The experimental datasets for this predictive model include nuclear radiation data and meteorological data collected from the entire country of Japan. Table 1 summarizes the statistics of the radiation and meteorological datasets.

**5.1.2 Evaluation Metrics.** We employed three widely used metrics, including Mean Absolute Error (MAE), Root Mean Squared Error (RMSE), and Mean Absolute Percentage Error (MAPE), for model evaluation. Lower values in MAE, RMSE, and MAPE indicate higher forecasting accuracy. Moreover, we follow [27, 48, 55] to discuss the

**Table 1: Statistic of radiation and meteorological datasets.**

|                        | Data Description |  | Japan-4H             | Japan-1D |
|------------------------|------------------|--|----------------------|----------|
| Nuclear radiation data | # of stations    |  | 3,841                | 3,841    |
|                        | # of timesteps   |  | 6,121                | 1,021    |
|                        | Interval         |  | 4 hour               | 1 day    |
| Meteorological data    | Time span        |  | 3/17/2021 - 1/1/2024 |          |
|                        | # of stations    |  | 235                  |          |
|                        | # of timesteps   |  | 24,483               |          |
|                        | Interval         |  | 1 hour               |          |
|                        | Time span        |  | 3/17/2021 - 1/1/2024 |          |

**Table 2: Evaluations of NRFormer and baselines on two real-world datasets.**

| Data     | Models          | 6th (24 hours / 6 days) |             |              | 9th (36 hours / 9 days) |             |              | 12th (48 hours / 12 days) |             |              | 24th (96 hours / 24 days) |             |              | sudden change |             |              |
|----------|-----------------|-------------------------|-------------|--------------|-------------------------|-------------|--------------|---------------------------|-------------|--------------|---------------------------|-------------|--------------|---------------|-------------|--------------|
|          |                 | MAE                     | RMSE        | MAPE         | MAE                     | RMSE        | MAPE         | MAE                       | RMSE        | MAPE         | MAE                       | RMSE        | MAPE         | MAE           | RMSE        | MAPE         |
| Japan-4H | HA              | 3.20                    | 19.73       | 3.18%        | 3.57                    | 20.16       | 3.58%        | 3.51                      | 20.20       | 3.48%        | 3.74                      | 20.78       | 3.64%        | 3.83          | 21.91       | 3.67%        |
|          | LR              | 2.80                    | 11.17       | 2.58%        | 2.96                    | 11.50       | 2.75%        | 2.94                      | 11.75       | 2.64%        | 3.04                      | 12.43       | 2.65%        | 3.44          | 14.19       | 2.88%        |
|          | XGBoost         | 2.38                    | 12.47       | 2.53%        | 2.49                    | 12.92       | 2.61%        | 2.58                      | 13.10       | 2.67%        | 2.80                      | 14.38       | 2.83%        | 3.64          | 16.46       | 2.97%        |
|          | DCRNN           | 2.15                    | 6.32        | 2.52%        | 2.30                    | 7.22        | 2.64%        | 2.42                      | 8.01        | 2.73%        | 2.79                      | 10.49       | 2.97%        | 3.09          | 12.12       | 2.81%        |
|          | STID            | 2.04                    | 5.72        | 2.47%        | 2.15                    | 6.18        | 2.56%        | 2.19                      | 6.50        | 2.59%        | 2.30                      | 7.51        | 2.63%        | 2.56          | 9.63        | 2.79%        |
|          | DLinear         | 2.12                    | 6.16        | 2.57%        | 2.20                    | 6.15        | 2.66%        | 2.22                      | 6.51        | 2.60%        | 2.31                      | 7.47        | 2.66%        | 2.35          | 8.99        | 2.62%        |
|          | PatchTST        | 1.89                    | 5.61        | 2.24%        | 2.01                    | 6.06        | 2.35%        | 2.05                      | 6.36        | 2.36%        | 2.23                      | 7.57        | 2.48%        | 2.32          | 7.84        | 2.47%        |
|          | Koopa           | 1.92                    | 5.69        | 2.28%        | 2.01                    | 6.08        | 2.35%        | 2.06                      | 6.42        | 2.38%        | 2.23                      | 7.64        | 2.55%        | 2.31          | 7.89        | 2.49%        |
|          | StemGNN         | 2.01                    | 6.11        | 2.72%        | 2.22                    | 6.19        | 2.52%        | 2.29                      | 6.47        | 2.55%        | 2.38                      | 7.53        | 2.59%        | 2.41          | 8.71        | 2.71%        |
|          | GWN             | 2.25                    | 5.99        | 2.78%        | 2.26                    | 6.30        | 2.72%        | 2.27                      | 6.48        | 2.70%        | 2.40                      | 7.33        | 2.80%        | 2.69          | 9.86        | 2.72%        |
| Japan-1D | LightCTS        | 1.87                    | 5.73        | 2.34%        | 2.01                    | 6.35        | 2.44%        | 2.15                      | 6.54        | 2.49%        | 2.29                      | 7.51        | 2.50%        | 2.40          | 8.69        | 2.68%        |
|          | <b>NRFormer</b> | <b>1.72</b>             | <b>4.82</b> | <b>2.07%</b> | <b>1.79</b>             | <b>5.15</b> | <b>2.14%</b> | <b>1.85</b>               | <b>5.39</b> | <b>2.18%</b> | <b>1.99</b>               | <b>6.24</b> | <b>2.31%</b> | <b>2.05</b>   | <b>6.76</b> | <b>2.31%</b> |
|          | HA              | 2.86                    | 17.83       | 2.73%        | 2.97                    | 18.22       | 2.86%        | 3.08                      | 18.58       | 2.98%        | 3.46                      | 20.01       | 3.45%        | 4.11          | 22.41       | 3.49%        |
|          | LR              | 2.46                    | 11.08       | 2.07%        | 2.55                    | 11.76       | 2.14%        | 2.67                      | 12.27       | 2.25%        | 2.95                      | 14.21       | 2.50%        | 3.79          | 13.92       | 3.01%        |
|          | XGBoost         | 2.51                    | 13.71       | 2.66%        | 2.64                    | 14.97       | 2.76%        | 2.73                      | 15.36       | 2.85%        | 2.95                      | 16.10       | 3.07%        | 3.82          | 15.14       | 3.15%        |
|          | DCRNN           | 1.97                    | 10.51       | 2.00%        | 2.14                    | 11.44       | 2.09%        | 2.78                      | 12.43       | 2.17%        | 2.64                      | 14.53       | 2.42%        | 3.46          | 13.63       | 3.02%        |
|          | STID            | 2.44                    | 7.42        | 3.41%        | 2.57                    | 7.93        | 3.58%        | 2.68                      | 8.38        | 3.72%        | 3.06                      | 9.99        | 4.23%        | 3.26          | 12.62       | 3.12%        |
|          | DLinear         | 1.89                    | 7.85        | 2.03%        | 2.11                    | 8.75        | 2.25%        | 2.19                      | 8.42        | 2.42%        | 2.33                      | 9.19        | 2.46%        | 2.48          | 10.54       | 2.60%        |
|          | PatchTST        | 1.84                    | 6.37        | 1.95%        | 1.97                    | 6.98        | 2.05%        | 2.03                      | 7.90        | 2.10%        | 2.17                      | 9.02        | 2.44%        | 2.44          | 9.92        | 2.53%        |
|          | Koopa           | 1.74                    | 7.03        | 2.00%        | 1.83                    | 7.68        | 2.10%        | 1.91                      | 8.17        | 2.15%        | 2.11                      | 9.77        | 2.49%        | 2.46          | 9.95        | 2.50%        |
|          | StemGNN         | 1.83                    | 7.79        | 2.11%        | 2.14                    | 8.63        | 2.23%        | 2.16                      | 8.39        | 2.42%        | 2.32                      | 9.13        | 2.43%        | 2.42          | 10.25       | 2.56%        |
|          | GWN             | 1.90                    | 7.31        | 2.16%        | 1.97                    | 7.77        | 2.19%        | 2.04                      | 8.15        | 2.26%        | 2.20                      | 9.19        | 2.43%        | 2.94          | 11.35       | 2.86%        |
| Japan-1D | LightCTS        | 1.85                    | 8.02        | 2.13%        | 1.93                    | 7.17        | 2.17%        | 2.00                      | 7.74        | 2.15%        | 2.15                      | 9.19        | 2.36%        | 2.39          | 9.97        | 2.51%        |
|          | <b>NRFormer</b> | <b>1.71</b>             | <b>6.25</b> | <b>1.90%</b> | <b>1.78</b>             | <b>6.82</b> | <b>1.94%</b> | <b>1.83</b>               | <b>7.28</b> | <b>1.98%</b> | <b>2.01</b>               | <b>8.76</b> | <b>2.13%</b> | <b>2.06</b>   | <b>8.97</b> | <b>2.21%</b> |

errors on predicting sudden changes. We identified the top 10% of samples in the test set with the greatest variation between observed and predicted values as sudden change samples for prediction. We provide detailed information on evaluation metrics in Appendix A.2.

**5.1.3 Baseline.** We compare the proposed NRFormer with 11 baseline methods, including Historical Average (HA) [51], XGBoost [5], Linear Regression (LR), DCRNN [25], Graph WaveNet [47], STID [35], DLinear [49], StemGNN [3], LightCTS [22], PatchTST [32] and Koopa [30]. We provide detailed baselines in Appendix A.1.

**5.1.4 Implementation Details.** The dataset was partitioned into three distinct subsets: 60% for training, 20% for validation, and 20% for testing. Our experiments are conducted on two different server configurations: Linux Centos with four RTX 3090 GPUs and Linux Ubuntu with two A800 GPUs. In terms of implementation, our model is implemented using PyTorch, with the Adam optimizer chosen for optimization. We set the learning rate and the weight decay to 0.001 and 0.0001, respectively. The batch size is fixed to 32. The number of temporal and spatial attention layers are fixed to 3, and the head of the multi-head attention module is set to 4.

## 5.2 Overall Performance

Table 2 presents the overall performance of NRFormer and all the baseline models on two real-world datasets with respect to MAE, RMSE, and MAPE. Overall, NRFormer consistently outperforms other baseline models on both datasets, demonstrating the effectiveness of NRFormer. Specifically, our model achieves improvements of 8.02%, 10.95%, 13.95%, and 13.1% beyond the LightCTS in terms of the MAE metric on 6, 9, 12, and 24 steps on the Japan-4H dataset, respectively. Similarly, the improvement of the MAE on the Japan-1D dataset is 7.57%, 7.77%, 8.5%, and 6.51%, respectively. Moreover, we can make the following observations: (1) All traditional methods (*i.e.*, HA, LR, and XGBoost) perform worse than deep learning models, as they fail to capture spatio-temporal patterns. (2) STGNN-based approaches (*i.e.*, DCRNN, Graph WaveNet) outperform HA, LR, and XGBoost by a large margin, indicating the

superiority of modeling intricate spatio-temporal dependencies. (3) STID performs worse than DCRNN and Graph WaveNet on Japan-1D dataset. The possible reason is that Japan-1D has fewer training samples than Japan-4H, which is insufficient to learn discriminative spatial and temporal identity embeddings. (4) LightCTS leverages a tailored designed automatic spatio-temporal feature extraction module and exhibits strong learning capabilities, achieving the best performance compared with other baseline models.

Moreover, compared to sudden change experiments, NRFormer shows substantial improvements across all datasets. Specifically, compared to Koopa in sudden change forecasting, NRFormer achieves an (11.25%, 14.32%, 7.23%) and (16.26%, 9.85%, 11.6%) improvement on the Japan-4H and Japan-1D datasets, respectively, under the MAE, RMSE, and MAPE metrics. The experimental results show that our model, by addressing spatiotemporal distribution imbalances and incorporating heterogeneous contextual factors, adapts more quickly to the non-stationary nature of radiation, providing more accurate predictions for sudden change samples.

## 5.3 Ablation Study

To verify the effectiveness of each component, we conduct ablation studies on four variants of the proposed NRFormer, including (1) *w/o normalization* removes non-stationary normalization and denormalization strategy, (2) *w/o temporal attention* replaces temporal attention layer by the linear layer, (3) *w/o spatial attention* removes the imbalance-aware spatial attention module, and (4) *w/o prompting* removes radiation propagation prompting module. The results of all variants are shown in Table 3.

As can be seen, NRFormer consistently outperforms all the variants, demonstrating the effectiveness of each proposed module. Specifically, the model performance degrades after removing the non-stationary normalization. This implies that incorporating instance-level normalization can attenuate the non-stationarity of radiation series and further enhance radiation forecasting accuracy. We observe that *w/o temporal attention* and *w/o spatial attention* perform worse than NRFormer, which indicates extracting the complex

**Table 3: Ablation studies of NRFormer on two datasets.**

| Dataset  | Models                           | MAE         | RMSE        | MAPE         |
|----------|----------------------------------|-------------|-------------|--------------|
| Japan-4H | w/o Normalization                | 2.16        | 6.68        | 2.53%        |
|          | w/o Temporal Attention           | 2.21        | 7.43        | 2.48%        |
|          | w/o Spatial Attention            | 2.24        | 7.36        | 2.50%        |
|          | w/o Prompting<br><b>NRFormer</b> | <b>1.99</b> | <b>6.24</b> | <b>2.31%</b> |
| Japan-1D | w/o Normalization                | 2.18        | 9.05        | 2.14%        |
|          | w/o Temporal Attention           | 2.25        | 9.68        | 2.44%        |
|          | w/o Spatial Attention            | 2.26        | 9.33        | 2.52%        |
|          | w/o Prompting<br><b>NRFormer</b> | <b>2.01</b> | <b>8.76</b> | <b>2.13%</b> |

spatio-temporal features in radiation series is critical for forecasting. Furthermore, we also observe that the contextual prompt has a significant impact on model performance, indicating the advance of modeling radiation propagation with external factors.

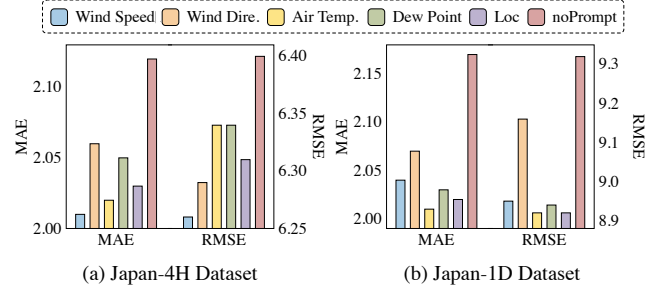
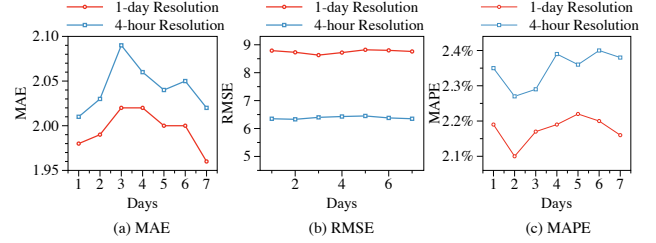
We also examine the utility of the contextual features we provide to the prompting module. *noPrompt* means that we remove all the contextual features from our framework. Others (e.g., Wind Speed) indicate using only one contextual feature. The results on MAE and RMSE are presented in Figure 7. In the absence of any contextual features, we separately add one feature at each time to assess its contribution. Here *noPrompt* indicates the performance of NRFormer without utilizing any additional contextual features. We can observe that incorporating each feature consistently improves the model performance beyond the *noPrompt*. In summary, the contextual features have a significant impact on nuclear radiation, and taking them into account is beneficial for forecasting.

#### 5.4 Deployed System Evaluation

To evaluate the real-world deployment performance of the NRFormer framework, we conducted a rigorous temporal generalization analysis using the most recent radiation monitoring data. As shown in Figure 8, the system maintained robust predictive capabilities during the critical evaluation window of January 25–31, 2025, achieving high accuracy in seven-day rolling averages despite significant temporal distributional shifts between the training period (March 17, 2021 – January 1, 2024) and the testing phase. This performance demonstrates the system's strong stability and robustness, thereby highlighting its practical utility for both individual users and government agencies by empowering them to make timely, data-driven decisions regarding emergency response and public safety.

### 6 RELATED WORKS

**Transformer.** The advent of the Transformer architecture [40] has been making a transformative impact across various fields, particularly in time series forecasting [4, 7, 11, 16, 42, 43, 56] and graph mining [6, 9, 24, 41, 45, 52, 57]. Transformer depends on self-attention mechanism to capture data correlations and is capable of modeling complicated and long-range dependencies. Due to the powerful capability, recently considerable endeavors have been made to adapt Transformer to time series and spatio-temporal data [10, 26, 27, 29, 50, 53]. For instance, by introducing a ProbSparse self-attention mechanism, Informer [56] enhances the Transformer framework for time series forecasting with high efficiency and scalability. As another example, Autoformer[44] further pushes the boundaries of time series forecasting by integrating decomposition

**Figure 7: Ablation study of each contextual feature.****Figure 8: Performance evaluation of deployed radiation forecasting system using recent data from January 25-31, 2025.**

and auto-correlation mechanism into Transformer. In this paper, we adapt the Transformer model with tailored designs to address the unique challenges in nuclear radiation forecasting.

**Spatial-temporal forecasting.** Spatio-temporal forecasting aims to predict the future states of spatio-temporal systems, such as traffic [10, 15, 17, 28] and atmospheric [12, 27] systems, based on historical observations. Nuclear radiation forecasting can be naturally modeled as a spatio-temporal forecasting problem. In recent years, Spatio-Temporal Graph Neural Networks (STGNNS) [14, 18, 36] has emerged as the most prevalent approaches in this field due to their strong capability in capturing intricate spatio-temporal dynamics. To name a few, DCRNN [25] models the diffusion process of traffic flows by leveraging graph-based diffusion convolution coupled with recurrent neural networks (RNNs). Graph Wavenet [47] learns an adaptive graph structure to capture the latent spatial relationships by decomposing the adjacency matrix into two learnable embedding matrices. In terms of radiation forecasting, existing studies rely on either numerical simulation [21] or statistical methods [8, 19, 39] to predict future radiation levels. However, these methods struggle with modeling complex spatio-temporal dependencies, leading to degraded performance in large-scale prediction scenarios.

### 7 CONCLUSION

In this paper, we introduce NRFormer, a spatio-temporal graph Transformer for national-wide nuclear radiation forecasting. Specifically, we first devise a non-stationary temporal attention module to capture the erratic and non-stationary characteristics in radiation time series. Subsequently, we propose an imbalance-aware spatial attention module to address the imbalanced spatial distribution issue by adaptively re-weighting the influence of stations from both macro-scale and proximity-constrained perspectives. Furthermore, a radiation propagation prompting module is developed to guide the predictive modeling process. Extensive experiments on real-world nuclear radiation datasets demonstrate the superiority of NRFormer against seven baselines. In the future, we plan to deploy NRFormer

to more countries so as to empower various decision-making tasks such as emergency response planning, thereby protecting environmental safety and public health.

## REFERENCES

- [1] Alan A Ager, Richard Lasko, Viktor Myroniuk, Sergiy Zibtsev, Michelle A Day, Uladzimir Usenia, Vadym Bogomolov, Ivan Kovalets, and Cody R Evers. 2019. The wildfire problem in areas contaminated by the Chernobyl disaster. *Science of the Total Environment* 696 (2019), 133954.
- [2] Lei Bai, Lina Yao, Can Li, Xianzhi Wang, and Can Wang. 2020. Adaptive graph convolutional recurrent network for traffic forecasting. *Advances in neural information processing systems* 33 (2020), 17804–17815.
- [3] Defu Cao, Yujing Wang, Juanyong Duan, Ce Zhang, Xia Zhu, Congrui Huang, Yunhai Tong, Bixiong Xu, Jing Bai, Jie Tong, et al. 2020. Spectral temporal graph neural network for multivariate time-series forecasting. *Advances in neural information processing systems* 33 (2020), 17766–17778.
- [4] Haizhou Cao, Zhenhao Huang, Tiechui Yao, Jue Wang, Hui He, and Yangang Wang. 2023. InPerformer: evolutionary decomposition transformers with interactive parallel attention for long-term time series forecasting. In *Proceedings of the AAAI Conference on Artificial Intelligence*, Vol. 37. 6906–6915.
- [5] Tianqi Chen and Carlos Guestrin. 2016. Xgboost: A scalable tree boosting system. In *Proceedings of the 22nd ACM SIGKDD International Conference on Knowledge Discovery and Data Mining*. 785–794.
- [6] Yuzhou Chen, Ignacio Segovia, and Yulia R Gel. 2021. Z-GCNETs: Time zigzags at graph convolutional networks for time series forecasting. In *International Conference on Machine Learning*, PMLR, 1684–1694.
- [7] Ranak Roy Chowdhury, Xiyuan Zhang, Jingbo Shang, Rajesh K Gupta, and Dezhong Hong. 2022. Tarnet: Task-aware reconstruction for time-series transformer. In *Proceedings of the 28th ACM SIGKDD Conference on Knowledge Discovery and Data Mining*. 212–220.
- [8] Stephen U Egarievwe, Jamie B Coble, and Laurence F Miller. 2016. Analysis of how well regression models predict radiation dose from the Fukushima Daiichi Nuclear Accident. *International Journal of Applied Physics and Mathematics* 6, 4 (2016), 150.
- [9] Yujie Fan, Mingxuan Ju, Shifu Hou, Yanfang Ye, Wenqiang Wan, Kui Wang, Yimeng Mei, and Qi Xiong. 2021. Heterogeneous temporal graph transformer: An intelligent system for evolving android malware detection. In *Proceedings of the 27th ACM SIGKDD Conference on Knowledge Discovery and Data Mining*. 2831–2839.
- [10] Aosong Feng and Leandros Tassoulas. 2022. Adaptive Graph Spatial-Temporal Transformer Network for Traffic Forecasting. In *Proceedings of the 31st ACM International Conference on Information and Knowledge Management*. 3933–3937.
- [11] Matt Gorbett, Hossein Shirazi, and Indrakshi Ray. 2023. Sparse binary transformers for multivariate time series modeling. In *Proceedings of the 29th ACM SIGKDD Conference on Knowledge Discovery and Data Mining*. 544–556.
- [12] Jindong Han, Hao Liu, Hengshu Zhu, Hui Xiong, and Dejing Dou. 2021. Joint air quality and weather prediction based on multi-adversarial spatiotemporal networks. In *Proceedings of the AAAI Conference on Artificial Intelligence*, Vol. 35. 4081–4089.
- [13] Jindong Han, Weijia Zhang, Hao Liu, and Hui Xiong. 2023. Machine Learning for Urban Air Quality Analytics: A Survey. *arXiv preprint arXiv:2310.09620* (2023).
- [14] Liangzhe Han, Bowen Du, Leilei Sun, Yanjie Fu, Yisheng Lv, and Hui Xiong. 2021. Dynamic and multi-faceted spatio-temporal deep learning for traffic speed forecasting. In *Proceedings of the 27th ACM SIGKDD Conference on Knowledge Discovery and Data Mining*. 547–555.
- [15] Jiahao Ji, Jingyuan Wang, Chao Huang, Junjie Wu, Boren Xu, Zhenhe Wu, Junbo Zhang, and Yu Zheng. 2023. Spatio-temporal self-supervised learning for traffic flow prediction. In *Proceedings of the AAAI conference on artificial intelligence*, Vol. 37. 4356–4364.
- [16] Yuxin Jia, Youfang Lin, Xinyan Hao, Yan Lin, Shengnan Guo, and Huaiyu Wan. 2024. WITRAN: Water-wave information transmission and recurrent acceleration network for long-range time series forecasting. *Advances in Neural Information Processing Systems* 36 (2024).
- [17] Renhe Jiang, Zhaonan Wang, Jiawei Yong, Puneet Jeph, Quanjun Chen, Yasumasa Kobayashi, Xuan Song, Shintaro Fukushima, and Toyotaro Suzumura. 2023. Spatio-temporal meta-graph learning for traffic forecasting. In *Proceedings of the AAAI conference on artificial intelligence*, Vol. 37. 8078–8086.
- [18] Guangyin Jin, Yuxuan Liang, Yuchen Fang, Zehzi Shao, Jincai Huang, Junbo Zhang, and Yu Zheng. 2023. Spatio-temporal graph neural networks for predictive learning in urban computing: A survey. *IEEE Transactions on Knowledge and Data Engineering* (2023).
- [19] SM Khanna, A Houdayer, A Jorio, C Carbone, M Parentean, and JW Gerdes. 1996. Nuclear radiation displacement damage prediction in gallium arsenide through low temperature photoluminescence measurements. *IEEE Transactions on Nuclear Science* 43, 6 (1996), 2601–2608.
- [20] Taesung Kim, Jinhee Kim, Yunwon Tae, Cheonbok Park, Jang-Ho Choi, and Jaegul Choo. 2021. Reversible instance normalization for accurate time-series forecasting against distribution shift. In *International Conference on Learning Representations*.
- [21] Yoon Hyuk Kim and Won Man Park. 2005. Use of simulation technology for prediction of radiation dose in nuclear power plant. In *Computational and Information Science: First International Symposium*. Springer, 413–418.
- [22] Zhichen Lai, Dalin Zhang, Huan Li, Christian S Jensen, Hua Lu, and Yan Zhao. 2023. LightCTS: A Lightweight Framework for Correlated Time Series Forecasting. *Proceedings of the ACM on Management of Data* 1, 2 (2023), 1–26.
- [23] Shiyong Lan, Yitong Ma, Weikang Huang, Wenwu Wang, Hongyu Yang, and Pyang Li. 2022. Dstagnn: Dynamic spatial-temporal aware graph neural network for traffic flow forecasting. In *International Conference on Machine Learning*, PMLR, 11906–11917.
- [24] Han Li, Dan Zhao, and Jianyang Zeng. 2022. KPGT: knowledge-guided pre-training of graph transformer for molecular property prediction. In *Proceedings of the 28th ACM SIGKDD Conference on Knowledge Discovery and Data Mining*. 857–867.
- [25] Yaguang Li, Rose Yu, Cyrus Shahabi, and Yan Liu. 2018. Diffusion Convolutional Recurrent Neural Network: Data-Driven Traffic Forecasting. In *International Conference on Learning Representations*.
- [26] Zhe Li, Shiyi Qi, Yiduo Li, and Zenglin Xu. 2023. Revisiting long-term time series forecasting: An investigation on linear mapping. *arXiv preprint arXiv:2305.10721* (2023).
- [27] Yuxuan Liang, Yutong Xia, Songyu Ke, Yiwei Wang, Qingsong Wen, Junbo Zhang, Yu Zheng, and Roger Zimmermann. 2023. Airformer: Predicting nationwide air quality in china with transformers. In *Proceedings of the AAAI Conference on Artificial Intelligence*, Vol. 37. 14329–14337.
- [28] Fan Liu, Hao Liu, and Wenzhao Jiang. 2022. Practical adversarial attacks on spatiotemporal traffic forecasting models. *Advances in Neural Information Processing Systems* 35 (2022), 19035–19047.
- [29] Hangchen Liu, Zheng Dong, Renhe Jiang, Jiewen Deng, Jinliang Deng, Quanjun Chen, and Xuan Song. 2023. Spatio-temporal adaptive embedding makes vanilla transformer sota for traffic forecasting. In *Proceedings of the 32nd ACM International Conference on Information and Knowledge Management*. 4125–4129.
- [30] Yong Liu, Chenyu Li, Jianmin Wang, and Mingsheng Long. 2024. Koopa: Learning non-stationary time series dynamics with koopman predictors. *Advances in Neural Information Processing Systems* 36 (2024).
- [31] Yong Liu, Haixu Wu, Jianmin Wang, and Mingsheng Long. 2022. Non-stationary transformers: Exploring the stationarity in time series forecasting. *Advances in Neural Information Processing Systems* 35 (2022), 9881–9893.
- [32] Yuqi Nie, Nam H Nguyen, Phanwadee Sinthong, and Jayant Kalagnanam. 2023. A Time Series is Worth 64 Words: Long-term Forecasting with Transformers. In *The Eleventh International Conference on Learning Representations*.
- [33] FangLi Qiao, GuanSuo Wang, Wei Zhao, JieChen Zhao, DeJun Dai, YaJuan Song, and ZhenYa Song. 2011. Predicting the spread of nuclear radiation from the damaged Fukushima Nuclear Power Plant. *Chinese Science Bulletin* 56 (2011), 1890–1896.
- [34] Zehzi Shao, Fei Wang, Yongjun Xu, Wei Wei, Chengqing Yu, Zhao Zhang, Di Yao, Guangyin Jin, Xin Cao, Gao Cong, et al. 2023. Exploring Progress in Multivariate Time Series Forecasting: Comprehensive Benchmarking and Heterogeneity Analysis. *arXiv preprint arXiv:2310.06119* (2023).
- [35] Zehzi Shao, Zhao Zhang, Fei Wang, Wei Wei, and Yongjun Xu. 2022. Spatial-temporal identity: A simple yet effective baseline for multivariate time series forecasting. In *Proceedings of the 31st ACM International Conference on Information and Knowledge Management*. 4454–4458.
- [36] Zehzi Shao, Zhao Zhang, Fei Wang, and Yongjun Xu. 2022. Pre-training enhanced spatial-temporal graph neural network for multivariate time series forecasting. In *Proceedings of the 28th ACM SIGKDD Conference on Knowledge Discovery and Data Mining*. 1567–1577.
- [37] Zehzi Shao, Zhao Zhang, Wei Wei, Fei Wang, Yongjun Xu, Xin Cao, and Christian S Jensen. 2022. Decoupled dynamic spatial-temporal graph neural network for traffic forecasting. *Proceedings of the VLDB Endowment* 15, 11 (2022), 2733–2746.
- [38] Georg Steinhauser, Alexander Brandl, and Thomas E Johnson. 2014. Comparison of the Chernobyl and Fukushima nuclear accidents: a review of the environmental impacts. *Science of the total environment* 470 (2014), 800–817.
- [39] Dajie Sun, Haruko Wainwright, Ishita Suresh, Akiyuki Seki, Hiroshi Takemiyia, and Kimiaki Saito. 2022. Spatial and temporal prediction of radiation dose rates near Fukushima Daiichi Nuclear Power Plant. *Journal of Environmental Radioactivity* 251 (2022), 106946.
- [40] Ashish Vaswani, Noam Shazeer, Niki Parmar, Jakob Uszkoreit, Llion Jones, Aidan N Gomez, Łukasz Kaiser, and Illia Polosukhin. 2017. Attention is all you need. *Advances in neural information processing systems* 30 (2017).
- [41] Dingsu Wang, Yuchen Yan, Ruizhong Qiu, Yada Zhu, Kaiyu Guan, Andrew Margenot, and Hanghang Tong. 2023. Networked time series imputation via position-aware graph enhanced variational autoencoders. In *Proceedings of the*

29th ACM SIGKDD Conference on Knowledge Discovery and Data Mining. 2256–2268.

[42] Huiqiang Wang, Jian Peng, Feihu Huang, Jince Wang, Junhui Chen, and Yifei Xiao. 2023. Micn: Multi-scale local and global context modeling for long-term series forecasting. In *The eleventh international conference on learning representations*.

[43] Haixu Wu, Tengge Hu, Yong Liu, Hang Zhou, Jianmin Wang, and Mingsheng Long. 2022. TimesNet: Temporal 2D-Variation Modeling for General Time Series Analysis. In *The Eleventh International Conference on Learning Representations*.

[44] Haixu Wu, Jiehui Xu, Jianmin Wang, and Mingsheng Long. 2021. Autoformer: Decomposition transformers with auto-correlation for long-term series forecasting. *Advances in Neural Information Processing Systems* 34 (2021), 22419–22430.

[45] Qitian Wu, Wentao Zhao, Zenan Li, David P Wipf, and Junchi Yan. 2022. Nodeformer: A scalable graph structure learning transformer for node classification. *Advances in Neural Information Processing Systems* 35 (2022), 27387–27401.

[46] Zonghan Wu, Shirui Pan, Guodong Long, Jing Jiang, Xiaojun Chang, and Chengqi Zhang. 2020. Connecting the dots: Multivariate time series forecasting with graph neural networks. In *Proceedings of the 26th ACM SIGKDD International Conference on Knowledge Discovery and Data Mining*. 753–763.

[47] Zonghan Wu, Shirui Pan, Guodong Long, Jing Jiang, and Chengqi Zhang. 2019. Graph wavenet for deep spatial-temporal graph modeling. *arXiv preprint arXiv:1906.00121* (2019).

[48] Xiwen Yi, Junbo Zhang, Zhaoyuan Wang, Tianrui Li, and Yu Zheng. 2018. Deep distributed fusion network for air quality prediction. In *Proceedings of the 24th ACM SIGKDD international conference on knowledge discovery & data mining*. 965–973.

[49] Ailing Zeng, Muxi Chen, Lei Zhang, and Qiang Xu. 2023. Are transformers effective for time series forecasting?. In *Proceedings of the AAAI conference on artificial intelligence*, Vol. 37. 11121–11128.

[50] Xuefan Zha, Wentao Zhu, Lv Xun, Sen Yang, and Ji Liu. 2021. Shifted chunk transformer for spatio-temporal representational learning. *Advances in Neural Information Processing Systems* 34 (2021), 11384–11396.

[51] Junbo Zhang, Yu Zheng, and Dekang Qi. 2017. Deep spatio-temporal residual networks for citywide crowd flows prediction. In *Proceedings of the AAAI conference on artificial intelligence*, Vol. 31.

[52] Weijia Zhang, Hao Liu, Lijun Zha, Hengshu Zhu, Ji Liu, Dejing Dou, and Hui Xiong. 2021. MugRep: A multi-task hierarchical graph representation learning framework for real estate appraisal. In *Proceedings of the 27th ACM SIGKDD conference on knowledge discovery & data mining*. 3937–3947.

[53] Yunhao Zhang and Junchi Yan. 2022. Crossformer: Transformer utilizing cross-dimension dependency for multivariate time series forecasting. In *The Eleventh International Conference on Learning Representations*.

[54] Zeyang Zhang, Xin Wang, Ziwei Zhang, Haoyang Li, Zhou Qin, and Wenwu Zhu. 2022. Dynamic graph neural networks under spatio-temporal distribution shift. *Advances in Neural Information Processing Systems* 35 (2022), 6074–6089.

[55] Yu Zheng, Xiwen Yi, Ming Li, Ruiyuan Li, Zhangqing Shan, Eric Chang, and Tianrui Li. 2015. Forecasting fine-grained air quality based on big data. In *Proceedings of the 21th ACM SIGKDD international conference on knowledge discovery and data mining*. 2267–2276.

[56] Haoyi Zhou, Shanghang Zhang, Jieqi Peng, Shuai Zhang, Jianxin Li, Hui Xiong, and Wancai Zhang. 2021. Informer: Beyond efficient transformer for long sequence time-series forecasting. In *Proceedings of the AAAI conference on artificial intelligence*, Vol. 35. 11106–11115.

[57] Wenhao Zhu, Tianyu Wen, Guojie Song, Liang Wang, and Bo Zheng. 2023. On Structural Expressive Power of Graph Transformers. In *Proceedings of the 29th ACM SIGKDD Conference on Knowledge Discovery and Data Mining*. ACM, 3628–3637.

## A SUPPLEMENTARY OF EXPERIMENT

### A.1 Baselines

In this section, we provide a brief overview of the baseline methods.

- HA [51]: A method predicts nuclear radiation levels by calculating the average value of historical readings for corresponding periods.
- XGBoost [5]: A method predicts nuclear radiation levels by leveraging an ensemble of decision trees, optimizing for both efficiency and performance.
- LR: A linear regression model that leverages the linear relationship between input variables and the output.
- DCRNN [25]: a spatio-temporal forecasting model that captures spatial dependencies through bidirectional random walks, while addressing temporal dependencies using encoder-decoder architecture with scheduled sampling.
- GWN [47]: A spatial-temporal graph modeling framework that generates an adaptive graph and integrates diffusion graph convolution with dilated causal convolution.
- STID [35]: A simple yet effective model for time series forecasting that only considers the historical time series with spatial-temporal identity embeddings.
- DLlinear [49]: This study introduces a surprisingly simple yet effective one-layer linear model, LTSF-Linear, which outperforms sophisticated Transformer-based long-term time series forecasting models across multiple datasets, challenging the prevailing reliance on complex Transformer architectures for temporal data analysis.
- StemGNN [3]: StemGNN is a novel framework that captures both inter-series correlations and temporal dependencies within multivariate time-series data in the spectral domain, using a combination of Graph Fourier Transform and Discrete Fourier Transform, thereby enhancing forecasting accuracy without relying on pre-defined priors.
- LightCTS [22]: LightCTS is a framework aimed at efficient, lightweight forecasting for correlated time series, balancing accuracy with reduced computational needs. It employs simplified operator stacking and innovative modules for better performance on resource-limited devices.
- PatchTST [32]: PatchTST is a Transformer-based model for multivariate time series forecasting, leveraging subseries patching and channel independence to reduce complexity and improve long-term accuracy, also excelling in self-supervised tasks and setting new accuracy benchmarks.
- Koopa [30]: Koopa introduces a novel approach for forecasting non-stationary time series by leveraging modern Koopman theory to disentangle and advance time-variant and time-invariant dynamics.

### A.2 Evaluation Metrics

We utilize three commonly adopted metrics to evaluate the performance of the model, namely Root Mean Squared Error (RMSE), Mean Absolute Error (MAE), and Mean Absolute Percentage Error (MAPE). These metrics are defined as follows. MAE, by contrast, measures the average magnitude of errors without considering their direction, offering a clear and straightforward interpretation

of overall accuracy:

$$MAE = \frac{1}{NK} \sum_{i=1}^N \sum_{j=1}^K |\hat{y}_{ij} - y_{ij}|. \quad (12)$$

RMSE calculates the square root of the average squared differences between predicted and observed values, thereby placing greater emphasis on larger errors:

$$RMSE = \sqrt{\frac{1}{NK} \sum_{i=1}^N \sum_{j=1}^K (\hat{y}_{ij} - y_{ij})^2}. \quad (13)$$

Meanwhile, MAPE expresses these errors as a percentage of the actual values, facilitating easier comparisons across different scales and datasets. Together, these metrics provide a comprehensive evaluation of the model's predictive capabilities and robustness:

$$MAPE = \frac{1}{NK} \sum_{i=1}^N \sum_{j=1}^K \left| \frac{\hat{y}_{ij} - y_{ij}}{y_{ij}} \right|, \quad (14)$$

where  $N$  and  $K$  are the number of station and future time steps, respectively.  $\hat{y}_{ij}$  denotes the future prediction and  $y_{ij}$  is the ground truth radiation level of station  $i$  at  $j$ -th time step.

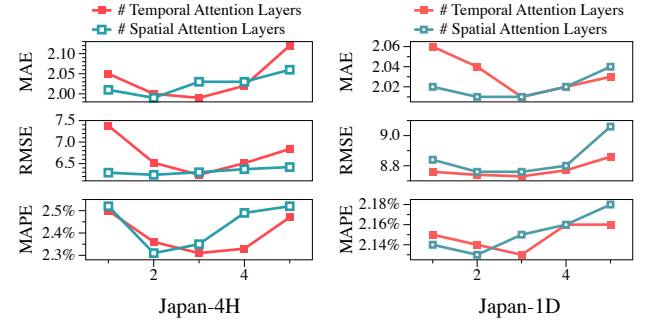
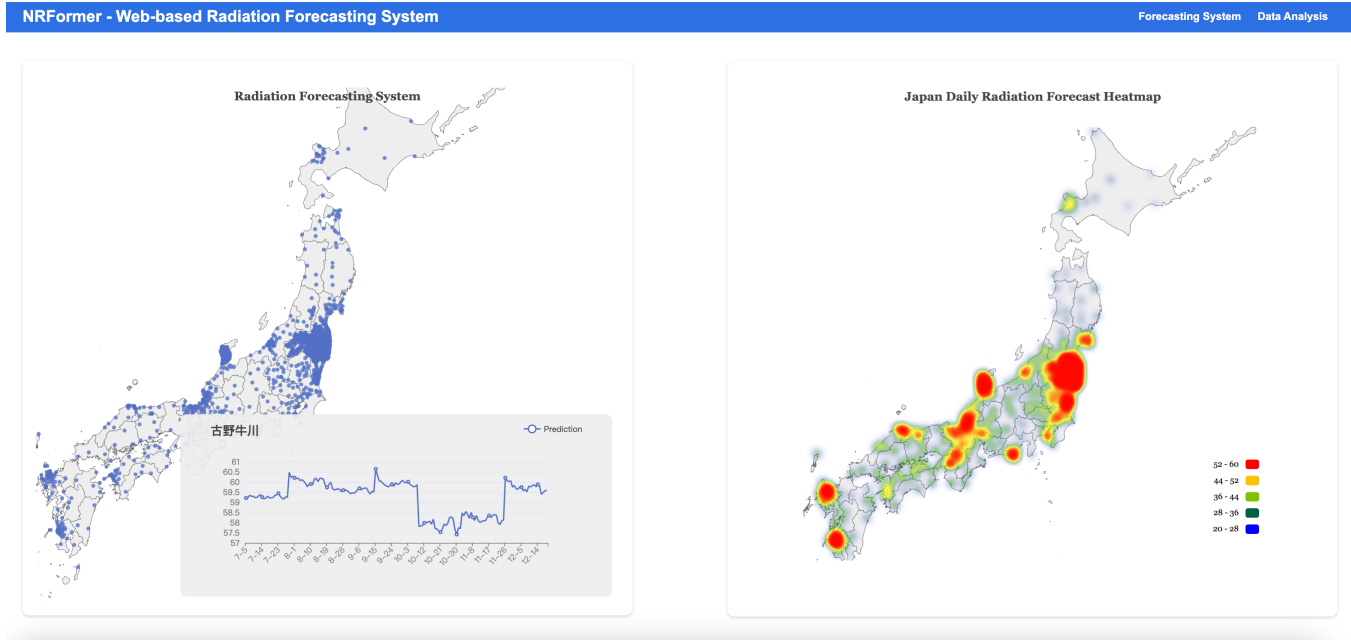


Figure 9: Parameter sensitivity of NRFormer.

### A.3 Parameter Sensitivity Analysis

We evaluate the impact of the number of temporal attention layers  $L_t$  and the number of spatial attention layers  $L_s$ . The results on MAE, RMSE, and MAPE are reported in Figure 9. First, we vary  $L_t$  from 1 to 5. As can be seen in Figure 9, the performance shows a fluctuation when increasing  $L_t$  from 1 to 3, and drops slightly by further increasing  $L_t$  from 3 to 5 on both Japan-4H and Japan-1D datasets. Overall, we achieve the best performance when setting  $L_t = 3$ . The possible reason is that a small  $L_t$  is insufficient to capture temporal correlation information, whereas too large  $L_t$  may introduce redundant and noisy information for our task, leading to performance degradation. We vary  $L_s$  from 1 to 5 and observe that our model achieves optimal performance when  $L_s$  is set to 2. Increasing or decreasing  $L_s$  beyond this point results in a decline in performance. This is primarily because a lower  $L_s$  fails to provide adequate spatio-temporal correlation of radiation propagation. Additionally, we noticed a performance drop when more spatial attention layers were added. This phenomenon might be caused by the fact that in an imbalanced spatial distribution scenario, using an excessive number of  $L_s$  can lead to overfitting, particularly for nodes with highly dense connections.



**Figure 10:** The deployed web-based radiation monitoring and forecasting system. Left panel: Forecasts for individual radiation monitoring stations, with interactive stations enabling users to access detailed predictions for the coming days. Right panel: Radiation dispersion dynamics across Japan, highlighting spatiotemporal propagation patterns over the next several days.

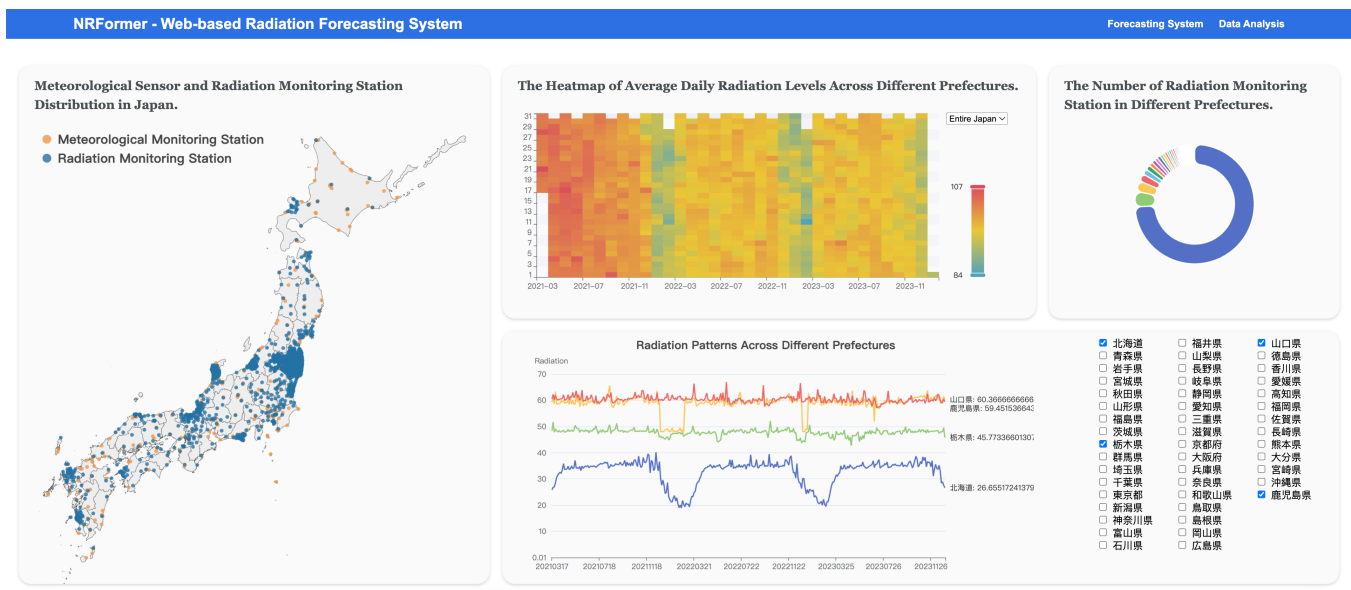


**Figure 11:** The data visualization of nuclear radiation in Japan: the left panel shows the distribution of radiation and meteorological monitoring stations; the top-center chart illustrates the average daily radiation levels across different prefectures; the top-right chart depicts the number of radiation monitoring stations in each prefecture; and the bottom-right chart presents temporal radiation patterns observed across various prefectures.